Electron optics of skewed micro-Einzel lenses

M. J. van Bruggen, B. van Someren, and P. Kruit[a)]
Delft University of Technology, Lorentzweg 1, 2628 CJ Delft, The Netherlands

(Received 29 September 2008; accepted 15 December 2008; published 21 January 2009)

Micro-Einzel lenses always suffer from chromatic and spherical aberration, even when the electron beam is exactly on the optical axis of the lens. When the inclination of the electron beam with respect to the lens axis increases, additional effects such as coma, astigmatism, and defocus start to dominate. An example of inclined electron beams in micro-Einzel lenses can be found in multi-electron-beam systems with a single source: the performance of a micro-Einzel lens array in front of a single Schottky electron source in a high brightness, high resolution multi-electron-beam scanning electron microscope is limited by its field aberrations. A model is presented to analyze the performance of inclined electron beams in micro-Einzel lenses. A first solution to improve this performance is to introduce micro-Einzel lenses of which the apertures are aligned with the center of the electron beam by shifting them perpendicular to the system optical axis, resulting in an array of skewed micro-Einzel lenses with reduced field aberrations. The model is used to prove the principles of this concept. A second solution is to fully compensate astigmatism and defocus by introducing elliptical lens holes with a diameter increasing with the off-axis distance. The presented solutions can be used to control the field aberrations of the multi-electron-beam system. © *2009 American Vacuum Society.* [DOI: 10.1116/1.3071850]

I. INTRODUCTION

Currently miniaturized electron-optical components made with microelectromechanical systems technology find their way into electron-optical systems.[1] This technology is particularly appropriate to make such components in an array,[2] which, for example, paves the way for improvement of throughput in maskless e-beam lithography or wafer inspection.[3–5] Various groups in the world are developing multi-electron-beam lithography systems based on a single source multiple path principle.[6–14] In the majority of these systems, microlens arrays are used to produce focused electron beams at the wafer or some intermediate plane in the system and they are often preceded by a collimator lens to ensure perpendicular incidence in the microlenses. In contrast to this sequence source—collimator-lens–microlens-array—it was proposed to position a microlens array directly in front of a source and use an array of deflectors to collimate the individual electron beams, with the advantage of avoiding field aberrations of the collimator lens.[15] Drawback of this setup is the inclined incidence in the microlenses, resulting in additional field aberrations. The effect of this inclined incidence on the microlens performance has been analyzed recently for aperture-type and two-electrode immersion-type microlenses.[16–18]

In this paper, the performance of the micro-Einzel lens type for inclined incidence of electron beams is analyzed. Solutions are presented to improve this performance by modifying the position, size, and shape of the micro-Einzel lens apertures. An analytical model is used to prove the concept.

In this paper, the case of inclined electron beams in micro-Einzel lenses is illustrated using a 100-beam scanning electron microscope (SEM) dedicated for high resolution electron beam induced deposition as an example. The source section of this system consists of a Schottky electron source with a micro-Einzel lens array (MELA) in front of it. This MELA produces an array of 100 virtual Schottky sources, which is imaged demagnified onto the sample surface by the SEM optics to obtain 100 1 nm diameter electron probes.

II. PERFORMANCE OF A STANDARD MELA FOR INCLINED ELECTRON BEAMS

The off-axis performance of a micro-Einzel lens is expected to become worse with increasing off-axis distance of the micro-Einzel lens. Especially the electron beams far from the system optical axis have a non-negligible inclined incidence in the micro-Einzel lens. This is illustrated with the 100 beam SEM case, of which the MELA geometrical, electrical, and optical parameters are listed in Table I. The dimensions of the MELA are determined from a fabrication point of view. The object and image side potentials are such that a standard Schottky electron source can be used with a field-free space between source and MELA. The half opening angle at the source side of each individual electron beam is such that the electron beam current is maximized at the sample surface. With a Schottky source reduced brightness of 5×10^{7} A m^{-2} sr^{-1} V^{-1} and a virtual source size of 30 nm, the resulting individual electron beam current is 24 pA. The distance between object plane and image plane of the MELA is set at approximately 30 mm for practical reasons. The MELA magnification in this example system is a direct consequence of the fact that the SEM magnetic lenses are used as pure focus or field lenses to reduce their field aberrations. Hence, with the magnification of these lenses fixed, the total system magnification must be set with the MELA magnifi-

a)Electronic mail: p.kruit@tudelft.nl

TABLE I. Geometrical, electrical, and optical parameters of the MELA in the 100 beam SEM example system.

Parameter	Value
Array size	10×10
Diameter of MELA apertures (μm)	160
Thickness of MELA electrodes (μm)	200
Distance between successive MELA electrodes (μm)	200
MELA pitch (μm)	240
Potential at object and image side (V)	5000
Focusing potential (V)	7200
Position object plane (mm)	−20.85
Lens midplane (mm)	1.90
Position image plane (mm)	10.14
Magnification	−0.362
Filling factor (%)	5.7
Half operating angle, source side (mrad)	0.20

cation. The filling factor is defined as the diameter of the electron beam at the MELA divided by the MELA aperture diameter.

With the parameters as given in Table I, it can be seen that the incidence angle of an electron beam in a micro-Einzel lens, calculated as the distance of that lens to the system optical axis divided by its object distance, can be up to 70 mrad. Then, the off-axis distance in parts of this lens is as large as 30% of the lens radius, which is three times its filling factor. The shift of a ray in the image plane caused by the third-order geometrical aberrations of the electrostatic micro-Einzel lens is calculated with the following expression:[19]

$$M^{-1}\Delta u_i^{(3)}(z_i) = S_{oa}\omega_a^2\bar{\omega}_a + 2K_{oa}\omega_a u_o\bar{\omega}_a + K_{oa}\omega_a^2\bar{u}_o + (F_{oa}+A_{oa})\omega_a u_o\bar{u}_o + A_{oa}u_o^2\bar{\omega}_a + D_{oa}u_o^2\bar{u}_o. \quad (1)$$

Here, $\Delta u_i^{(3)}(z_i)$, ω_a, and u_o are the complex notations for the shift in the image plane caused by third-order geometrical aberration, the electron beam half angle, and the position in the object plane respectively. Note that an off-axis position u_o of the electron beam in the object plane in combination with an on-axis micro-Einzel lens is equivalent to an axial electron beam traveling through a micro-Einzel lens at a position u_o off axis. The definitions are as follows: $\Delta u_i^{(3)}(z_i) = \Delta x_i^{(3)} + i\Delta y_i^{(3)}$, $\omega_a = \alpha_x + i\alpha_y$, and $u_o = x_o + iy_o$ where $\Delta x_i^{(3)}$ and $\Delta y_i^{(3)}$ are the third-order geometrical aberrations in the image plane in the x and y directions, respectively, while α_x, α_y, x_o, and y_o are the electron-beam half angle and position in the object plane in x and y directions, respectively. The coefficients S_{oa}, K_{oa}, A_{oa}, F_{oa}, and D_{oa} at the object side for spherical aberration, coma, astigmatism, field curvature, and distortion, respectively, are for a specified aperture position in the z direction along the optical axis. This aperture position is indicated in Fig. 1. The coefficients are calculated with ELD.[20] The chromatic aberrations can also be expressed in terms of the complex electron beam half angle and position in the object plane:[19]

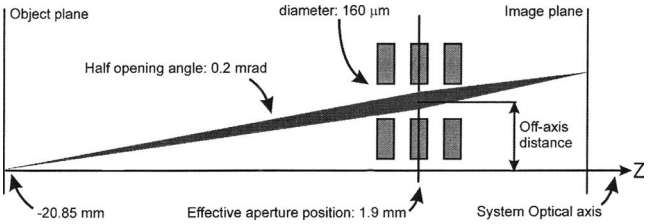

FIG. 1. Schematic overview of skewed incidence of an electron beam in an off-axis micro-Einzel lens (not to scale). In Fig. 2, the FW50 aberration disk is plotted vs the off-axis distance of the micro-Einzel lens for aperture position of 1.9 mm, to show the poor off-axis performance. In Fig. 3, the FW50 aberration disk is plotted vs aperture position for off-axis distance 1.1 mm.

$$M^{-1}\Delta u_i^{(c)}(z_i) = [X_{oa}\omega_a + T_{oa}u_o]\frac{\Delta U_{50}}{U_r}. \quad (2)$$

Here, $\Delta u_i^{(c)}(z_i)$ is the complex notation for the shift in the image plane caused by first-order chromatic aberration. It is defined as $\Delta u_i^{(c)}(z_i) = \Delta x_i^{(c)} + i\Delta y_i^{(c)}$, where $\Delta x_i^{(c)}$ and $\Delta y_i^{(c)}$ are the first-order chromatic aberrations in the image plane in the x and y directions respectively. The coefficients X_{oa} and T_{oa} for axial chromatic aberration and transversal chromatic aberration, respectively, are defined on the object side and again for a specified aperture position. They are also found with ELD.[20] Finally U_r is the relativistically corrected electron energy and ΔU_{50} the associated FW50 energy spread. For a specified object position, electron-beam half angle, and aperture position, the corresponding FW50 aberration disk in the MELA image plane is then found after calculating the shifts in the image plane for typically 500 electrons that are uniformly distributed in the micro-Einzel lens entrance plane, taking into account only the third-order geometrical aberrations. An overview of a skewed electron beam in an off-axis micro-Einzel lens is shown in Fig. 1. In Fig. 2, the FW50 aberration disk is shown as a function of the off-axis distance in the object plane. This is done for the optical parameters as indicated in Table I. For increasing off-axis distance, the contributions of astigmatism and field curvature to the FW50 aberration disk start to dominate and a quadratic dependency is observed. For the maximum off-axis distance of 4.5×240 μm and lens pitch=1.1 mm, the FW50 aberration disk in the MELA image plane is approximately 74 nm, while the geometrical spot size is 11 nm. In Fig. 3, the FW50 aberration disk is plotted as a function of the aperture position along the optical axis for a fixed maximum off-axis distance of 1.1 mm. A clear optimum is observed at the coma-free aperture position along the optical axis of approximately 1.9 mm.[21] This was already used in the analysis of inclined electron beams in two-electrode lenses.[16] At this coma-free aperture position, which coincides with the lens midplane for this symmetric lens, the coma and transversal chromatic aberration are zero, the distortion is small, and the astigmatism and field curvature show a minimum. This can be seen in Fig. 4 where the third, fourth, and fifth terms of Eq. (1) and

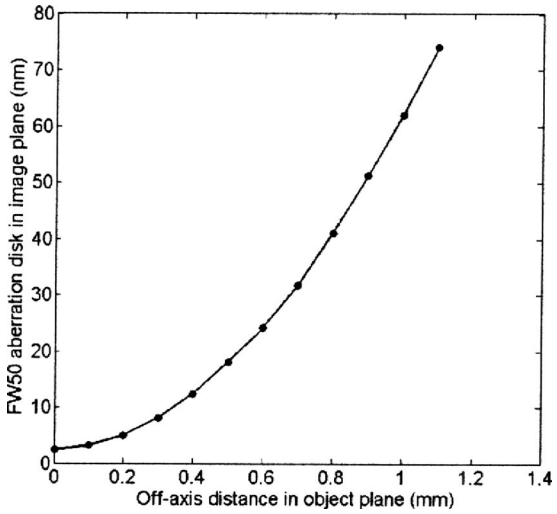

FIG. 2. FW50 aberration disk of the 160 μm diameter micro-Einzel lens in its image plane caused by third-order geometrical aberrations vs the off-axis distance of an electron beam in the object plane. The aperture position is at 1.9 mm and the beam half angle is 0.2 mrad.

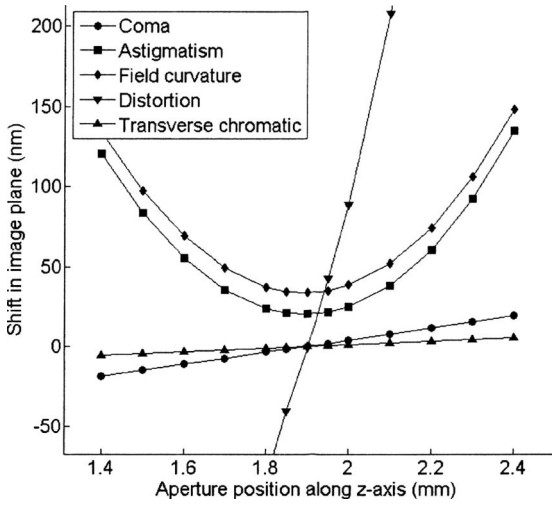

FIG. 4. Aberration contributions in the image plane of the micro-Einzel lens as a function of the (virtual) aperture position along the optical axis. A coma-free aperture position is observed.

the second term of Eq. (2) are plotted as a function of the aperture position. This coma-free aperture position along the optical axis for each individual micro-Einzel lens is translated to a corresponding position of a current-limiting aperture in the X-Y plane. The accuracy of these current-limiting aperture positions must then be better than 1 μm, which can be achieved with a focused ion beam milling tool.

Even with the current-limiting aperture positions such that the electron beams are traveling coma-free through the MELA, the contributions of astigmatism and field curvature are unacceptably large compared with the geometrical image of the Schottky electron source, especially for electron beams with large off-axis distance at MELA. The conclusion is that this problem must be solved. Two possible solutions are proposed in the next two sections. In Sec. III, the concept of a skewed micro-Einzel lens is presented, and in Sec. IV, compensation of field curvature and astigmatism of the MELA with modified micro-Einzel lens aperture shapes is explained.[22]

III. SKEWED MICRO-EINZEL LENSES

The previous section showed the presence of astigmatism and field curvature for especially far off-axis electron beams. These electron beams travel inclined through their corresponding micro-Einzel lens as shown in Fig. 5(a). The hypothesis proposed here is that such a micro-Einzel lens can be considered as a set of three separate lenses approximately situated at the three lens electrodes: For this specific accelerating micro-Einzel lens, these are two positive lenses at the outside and a negative lens in the center. In the case of coma-

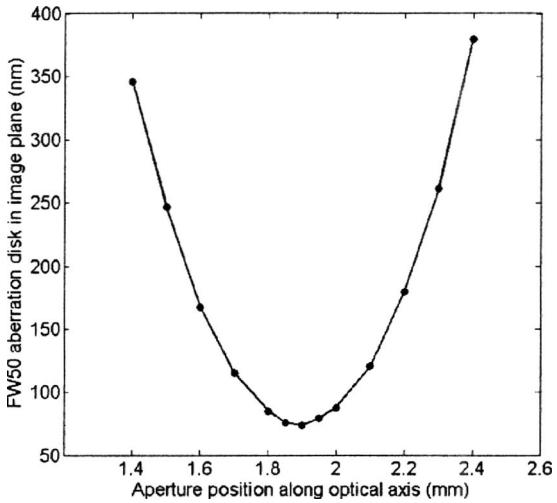

FIG. 3. FW50 aberration disk of the 160 μm diameter micro-Einzel lens in its image plane caused by third-order geometrical aberrations vs the aperture position along the optical axis. The off-axis distance of the electron beam in the object plane is 1.1 mm and the beam half angle is 0.2 mrad.

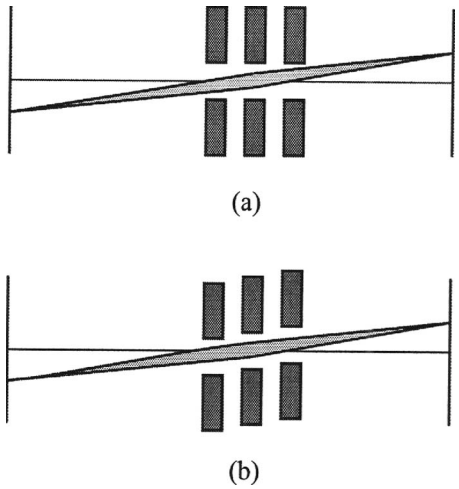

FIG. 5. (a) Standard micro-Einzel lens: off-axis electron beams travel skewed through this lens. (b) Skewed micro-Einzel lens: the idea is to reduce the off-axis aberrations in the two outer lens parts by shifting the corresponding electrodes.

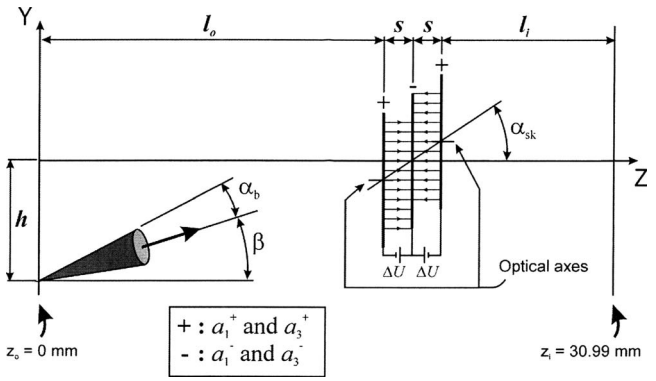

FIG. 6. Analytical model of the micro-Einzel lens: this lens is represented by three thin lenses with mutual distance s described by a first-order and a third-order coefficient (indicated in the box). The coefficients of the central negative lens are related to the coefficients of the two positive lenses by two proportionality factors. In addition, there is an accelerating and decelerating field between the lenses as shown, with associated potential difference ΔU. The distance between object plane and first thin lens is l_0 and between last thin lens and image plane l_i. The four lens parameters, l_0, s, and ΔU are fitted to ELD data. The electron beam starts a distance h off axis with beam half angle α_b and elevation angle α_{el} with respect to the optical axis. The micro-Einzel lens skewing angle is indicated by α_{sk}.

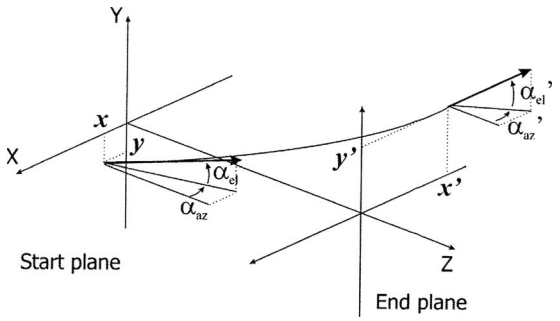

FIG. 7. Electron trajectory in a decelerating field. Note the definition of the azimuth and elevation angles α_{az} and α_{el}.

free incidence, the astigmatism and field curvature are then introduced in the outer lens parts. A quick analysis shows that the height of incidence in these parts is approximately three times larger than the electron beam radius for a micro-Einzel lens at 1.1 mm off-axis distance. The solution presented in this section is to shift the two outer electrodes as shown in Fig. 5(b) to minimize the field aberrations caused by the outer lens parts. In the forthcoming, this type of micro-Einzel lens is called a skewed micro-Einzel lens.

A. Analytical model of the micro-Einzel lens

The properties of the skewed micro-Einzel lens cannot be calculated by the aforementioned finite element program ELD as this only calculates the fields for rotationally symmetric systems.[20] With electrode shifts larger than 5% of the diameter of the lens aperture, tolerance packages are also not appropriate. For this specific problem, a full three-dimensional calculation of the electrostatic potential seems to be required. However, to prove both the hypothesis and the concept of the skewed micro-Einzel lens, the construction of a relatively simple analytical model is an attractive alternative. The proposed micro-Einzel lens consists of three electrodes of 200 μm thickness at 200 μm spacing with 160 μm circular apertures. It can thus be considered as a thick symmetric lens. As seen from the object side, the proposed model of this lens consists of a positive thin lens, an accelerating field, a negative thin lens, a decelerating field, and again a positive thin lens. A schematic overview of the model is shown in Fig. 6. The first-order properties of the thin lenses are described by lens strength a_1^+ of the two positive lenses and lens strength a_1^- of the negative lens, while the third-order properties are described by a_3^+ and a_3^-, the third order geometrical aberration coefficients for the two positive lenses and the negative lens, respectively. They are defined as

$$\Delta\alpha_i = a_1 h + a_3 h^3. \tag{3}$$

Here, $\Delta\alpha_i$ is the angular deviation at the thin lens and h the off-axis distance in the thin lens. By symmetry, the parameters of the two positive lenses are equal. The micro-Einzel lens is then fully described by a set of two first-order and two third-order parameters, the position s of the two positive thin lenses with respect to the negative thin lens, and a potential difference ΔU associated with the accelerating and decelerating fields in between these thin lenses. An electron beam then starts at an off-axis distance h in the negative y direction in the object plane with electron-beam half angle α_b and elevation angle β with respect to the optical axis. The object plane on its turn is at a distance l_o from the first thin lens and, with the data in Table I, the image plane is at 20.85+10.14 =30.99 mm from the object plane.

Electron trajectories inside the electron beam are obtained in subsequent steps with (1) propagation in drift space from object plane to first thin lens and from last thin lens to the image plane, which is a straightforward calculation, (2) angular deviation at the thin lenses which is calculated using a two-dimensional version of Eq. (3), and (3) the calculation of the change in position and angle caused by the accelerating and decelerating fields in between the thin lenses. This situation is sketched in Fig. 7. With x, y, α_{az}, and α_{el} the position in the x and y directions and azimuth and elevation angles in the start plane, the corresponding positions and angles in the end plane, denoted by primes, are found with

$$\begin{pmatrix} x' \\ \alpha'_{az} \\ y' \\ \alpha'_{el} \end{pmatrix} = T \begin{pmatrix} x \\ \alpha_{az} \\ x \\ \alpha_{el} \end{pmatrix}, \tag{4}$$

with T the transfer matrix:

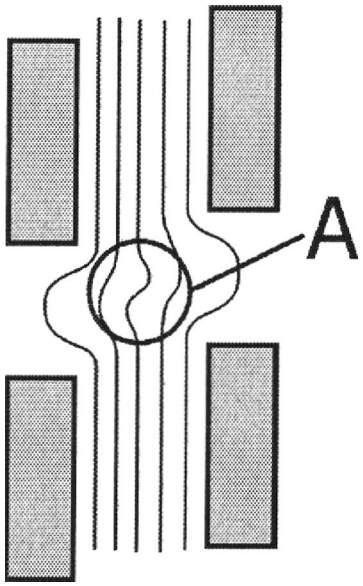

FIG. 8. Cross-sectional view of two electrodes of a skewed lens and the equipotential planes. The specific shape of the electrostatic field and the effect it has on an electron beam are not taken into account in the analytical model presented here.

$$T = \begin{pmatrix} 1 & \dfrac{-2s}{1+q^{1/2}} & 0 & 0 \\ 0 & q^{-1/2} & 0 & 0 \\ 0 & 0 & 1 & \dfrac{2s}{1+q^{1/2}} \\ 0 & 0 & 0 & q^{-1/2} \end{pmatrix}. \tag{5}$$

Here, q is defined as

$$q = \begin{cases} 1 + \dfrac{\Delta U}{U_{\mathrm{ex}}}, & \text{for the accelerating field} \\ \left(1 + \dfrac{\Delta U}{U_{\mathrm{ex}}}\right)^{-1}, & \text{for the decelerating field.} \end{cases} \tag{6}$$

Here, U_{ex} is the extractor potential of the Schottky electron source. In the model, the two positive thin lenses can be shifted in the y direction such that a skewed lens with skewing angle α_{sk} is introduced. The expectation is that for a specific off-axis height h, the optimum skewing angle is equal to the electron beam elevation angle that would have given coma-free incidence. The four lens parameters a_1^+, a_1^-, a_3^+, and a_3^- and l_o, s, and ΔU are found in a fitting process described in the next section.

One of the limitations of the model is the description of the electrostatic field in between the thin lenses by accelerating and decelerating fields. Especially with the introduction of a skewed lens, the real shapes of the equipotential planes in between the electrodes are not flat as suggested in the model, but instead their cross section shows an s shape (see detail A in Fig. 8). The effect this has on passing electrons is not taken into account in the presented model. However, the goal of this model is to prove that by skewing a micro-Einzel lens, the field curvature and astigmatism as observed in Fig. 2 can be reduced. For this purpose, the model is expected to be appropriate.

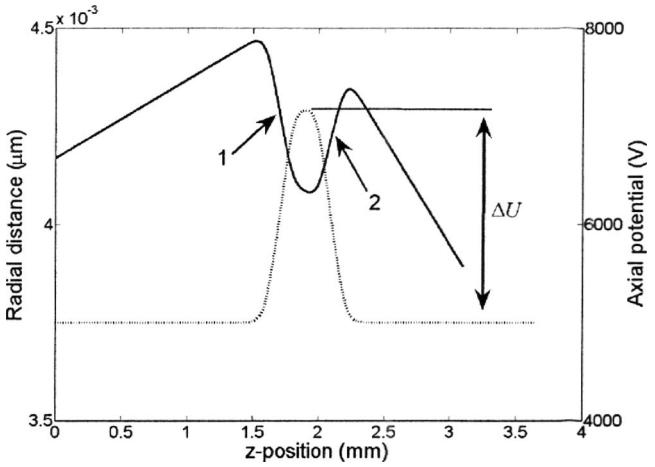

FIG. 9. Part of an electron trajectory starting on axis in the object plane (solid line) obtained with ray tracing program TRASYS (Ref. 23) and the axial potential (dotted line) as obtained with ELD (Ref. 20). From these data, the values of the model parameters l_0, s, and ΔU are obtained.

B. Method of parameter fitting

The lens-specific input parameters for the analytical model are lens strengths a_1^+ and a_1^-, third-order coefficients a_3^+ and a_3^-, distances l_o and s, and potential difference ΔU. The parameters l_o, s, and ΔU are first obtained using an electron trajectory calculated with ray tracing program TRASYS (Ref. 23) and the axial potential resulting from ELD.[20] They are shown in Fig. 9. By calculating the two crossing points of the two asymptotes in object and image space with the tangents to the points 1 and 2 and the single crossing point between that of the two tangents, l_o and s are found. For the value of ΔU, the difference between the maximum and minimum axial potential is chosen. With these three parameters and the set a_1^+, a_1^-, a_3^+, and a_3^-, the model calculates four different electron trajectories for the fitting process: (1) two electrons starting at an off-axis distance of 5 μm parallel to the axis, one with and the other without third-order contributions, and (2) two electrons starting on-axis in the object plane with elevation angle 0.2 mrad with respect to the optical axis, again one with and the other without third-order contributions. The output is the object position z_i, the magnification M and the coefficients of spherical aberration $C_s(M)$ and $C_s(0)$ at the image side at magnification M and zero, respectively. The parameters a_1^+, a_1^-, a_3^+, and a_3^- are then obtained by fitting the model output to the corresponding output resulting from ELD.[20] The fitting process is depicted schematically in Fig. 10.

C. Results

The resulting model parameters obtained in the fitting process described in the previous section are presented in Table II. In Table III, the corresponding output of both the

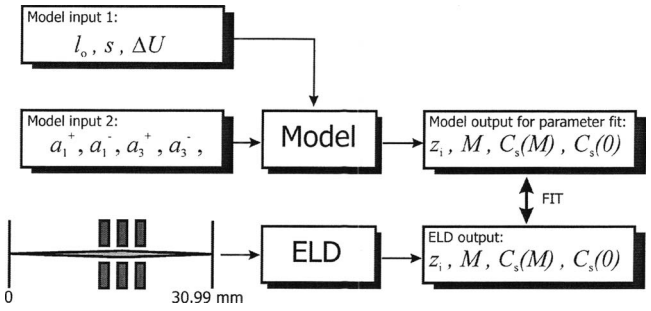

FIG. 10. Schematic representation of the fitting process.

model and ELD are shown. With these model parameters, the FW50 aberration disk is obtained for an electron beam with specified object position, electron-beam half angle, and elevation angle with respect to the optical axis by calculating the shifts in the image plane for approximately 500 electrons that are uniformly distributed in the micro-Einzel lens entrance plane. This method is identical to that used in Sec. II to calculate the FW50 disks with ELD aberration coefficients. This is first done for a zero micro-Einzel lens skewing angle for varying electron beam off-axis distance in the object plane. The results are presented in Fig. 11. The obtained data for the nonskewed lens (square markers) are compared with the results obtained with ELD (round markers). This curve is identical to the one presented in Fig. 2. In the same figure, the result for the skewed lens is presented, showing a clear decrease of the FW50 aberration disk in the image plane. In all cases, the electron-beam elevation angle with respect to the axis is optimized to give a coma-free minimum FW50 aberration disk. For the skewed micro-Einzel lens, the FW50 aberration disk for the electron beam with 1.1 mm maximum off-axis distance in the object plane and beam half angle of 0.2 mrad is determined as a function of the skewing angle to show the optimum at a skewing angle equal to the electron-beam elevation angle with respect to the optical axis of $h/(l_o+s)=48.35$ mrad with h of 1.1 mm. This result is shown in Fig. 12. Finally, for this same off-axis electron beam, cross sections are plotted in Fig. 13 for varying position along the optical axis, ending with the electron-beam cross section in the image plane. This is done for the nonskewed micro-Einzel lens (a), the skewed micro-Einzel lens (b), and the skewed micro-Einzel lens excluding third-order aberrations (c).

TABLE II. Fitted model parameters.

Parameter	Value
l_o (mm)	22.44
s (mm)	0.309 8
ΔU (V)	2166
a_1^+ (1/mm)	0.369 7
a_3^+ (1/mm^3)	1.322
a_1^+ (1/mm)	–0.517 58
a_3^- (1/mm^3)	2.644

TABLE III. Results of the fitting process.

Parameter	ELD	Model
z_i (mm)	30.99	30.99
M	–0.3624	–0.3627
$C_s(M)$ (mm)	2.046×10^4	2.046×10^4
$C_s(0)$ (mm)	5.946×10^3	5.946×10^3

D. Discussion and conclusion

The micro-Einzel lens treated in this chapter was considered as a thick lens consisting of three distinct electrostatic lens fields with positive, negative, and positive strengths, respectively. The hypothesis was that field aberrations are introduced in the outer parts of the lens when off-axis electron beams travel skewed through it. This micro-Einzel lens was modeled as a set of three thin lenses arranged as follows: positive-negative-positive. Accelerating and decelerating fields in between these thin lenses were taken into account. The results obtained with this model actually prove the proposed hypothesis: At coma-free incidence of the electron beam in a standard micro-Einzel lens, the remaining contributions are astigmatism and field curvature [Fig. 13(a)] which increase with off-axis distance in the object plane (Fig. 11, square markers). The results are in good agreement with ELD, although a large sensitivity was observed for small variations in the input parameters of the model. The next obvious step is to skew the lens around the electron beam, and it is expected that in order to obtain an optimum result, it must be done in such a way that the skewing angle of the micro-Einzel lens is equal to the elevation angle of the electron beam with the optical axis. This is confirmed by the results presented in Fig. 12: the FW50 aberration disk decreases from 74 nm for a nonskewed lens, corresponding with point A in Fig. 11 to approximately 16 nm at point B for a micro-Einzel lens with a skewing angle equal to the elec-

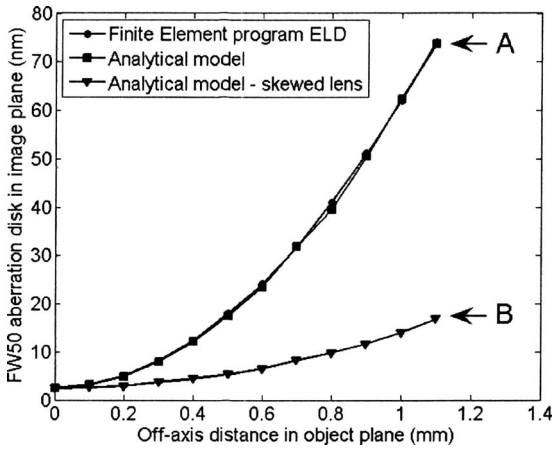

FIG. 11. FW50 aberration disk in the image plane caused by third-order geometrical aberrations vs off-axis distance for an electron beam with 1.1 mm maximum off-axis distance and half angle 0.2 mrad. The improvement obtained by skewing the micro-Einzel lens is apparent. Electron-beam cross-section series at varying z position for A and B in Fig. 13 show the presence of field curvature and astigmatism.

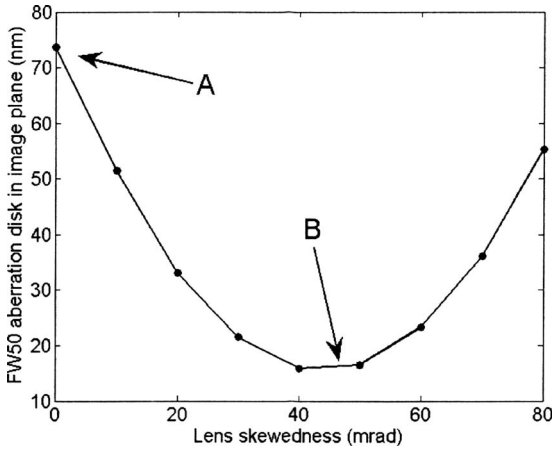

FIG. 12. FW50 aberration disk in the image plane caused by third-order geometrical aberrations vs the lens skewing angle for an electron beam with 1.1 mm maximum off-axis distance and half angle 0.2 mrad. The FW50 aberration disk decreases from 74 nm for a nonskewed lens (point A in Fig. 11) to approximately 16 nm for a lens skewing angle equal to the electron beam elevation angle with respect to the axis.

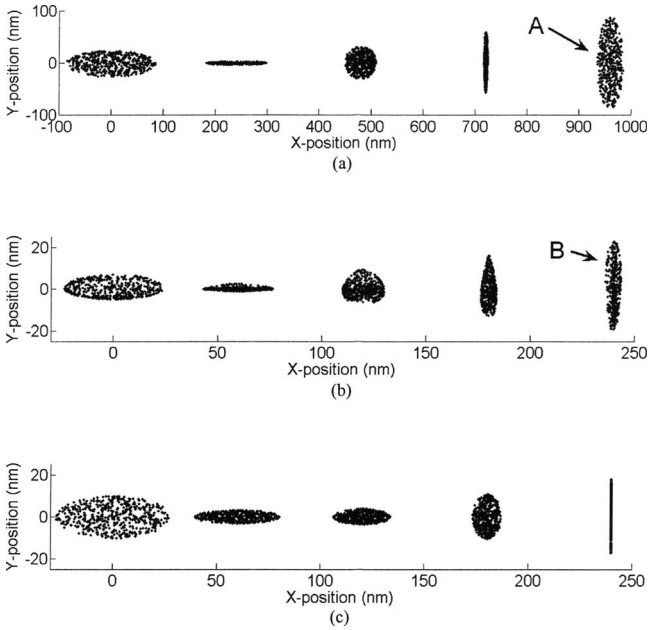

FIG. 13. Electron-beam cross sections for varying position along the optical (z) axis for an electron beam with maximum off-axis distance of 1.1 mm in the object plane, half opening angle of 0.2 mrad, and elevation angle of 48.35 mrad: (a) for zero skewing angle and distance Δz between neighboring cross sections of 50 μm, (b) for a skewing angle of 48.35 mrad and $\Delta z=12.5$ μm, and (c) for a skewing angle of 48.35 mrad, $a_3^+=0$, and $\Delta z=12.5$ μm. The rightmost beam cross section is in the image plane: astigmatism and field curvature is clearly present for all three cases. Note the difference in scale: the skewed micro-Einzel lens gives an improvement in FW50 aberration disk of approximately a factor of 4.5. The latter series shows astigmatism caused by a nonperpendicular lens plane with respect to the electron beam axis and is also present in the absence of third-order aberration in the model. Note that the cross sections are shifted in the x-direction to display them in a single plot.

tron beam elevation angle with respect to the axis. In this case, the off-axis incidence in each of the three thin lenses in the model is zero. Even then a clear astigmatism and field curvature effect are observed in the sequence of electron-beam cross sections in Fig. 13(b), corresponding with point B in Fig. 11. This astigmatism is a first-order effect. Its presence is explained by examining the situation in Fig. 14: It shows a thin lens which is rotated over skewing angle α_{sk} around an axis parallel to the axis. Focusing on the electron trajectories 1–4 parallel to the axis at equal off-axis distance and with z-axis crossing points z_1, z_2, and $z_3=z_4$, the variations $\Delta f_{sh}=z_1-z_2$ and $\Delta f_{as}=z_3-z_2$ can be found in a straightforward way:

$$\frac{\Delta f_{sh}}{f}=2\alpha_{sk}\alpha_b, \tag{7}$$

$$\frac{\Delta f_{as}}{f}=\frac{1}{2}\alpha_{sk}^2. \tag{8}$$

Here, the variations are denoted relative to the lens focal distance f and α_b is the electron-beam half angle. With $\alpha_{sk} \gg \alpha_b$, the introduction of astigmatism is the obvious result. This can be seen in Fig. 13(c) showing the same sequence of beam cross sections as in Fig. 13(b) but without the third-order contributions. Note that the difference between the two series is exactly the spherical aberration.

The astigmatism and corresponding field curvature resulting from first-order optics are still unacceptably large. It is concluded here that other methods are required to reduce astigmatism and field curvature. These are treated in the next section.

IV. MICRO-EINZEL LENSES WITH MODIFIED APERTURE SHAPE AND SIZE

In this section, the compensation of MELA field aberrations by modifying its electrode shapes and sizes is discussed. Here, focus is on astigmatism and field curvature, as from the previous sections, these turned out to be the main contributors to the spot size for large electron-beam inclination. Field curvature of the micro-Einzel lens is corrected by introducing a variation of the diameter $D_E(h)$ of all three electrodes of the micro-Einzel lenses according to[22]

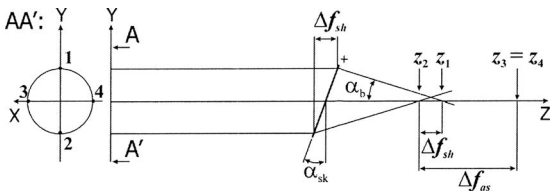

FIG. 14. Electron trajectories 1–4 with equal off-axis distance through a thin lens rotated over angle α_{sk} around an axis parallel to the x axis. The crossing points with the z axis are z_1, z_2, z_3, and z_4. From first-order optics, it follows that $z_3=z_4$ (Gaussian image plane) and $z_3-z_2>z_3-z_1\gg z_1-z_2$. This results in astigmatism.

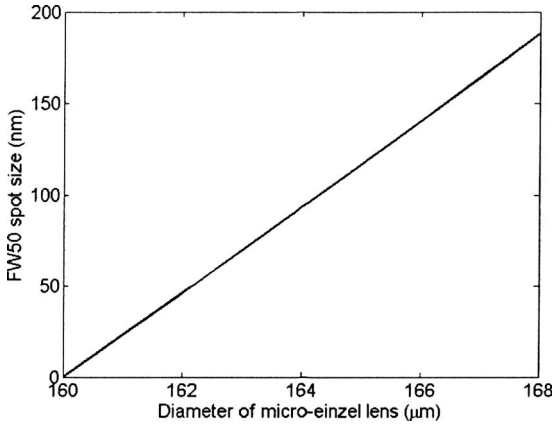

FIG. 15. FW50 spot size as a function of the diameter of the micro-Einzel lens from calculations with ELD (Ref. 20). This is the result of a defocus caused by the decreasing micro-Einzel lens strength at increasing diameter. Note that for a diameter of 160 μm, the FW50 spot size is zero.

$$D_E(h) = D_E(0) + Kh^2, \quad K > 0. \tag{9}$$

Here, $D_E(0)$ is the axial lens diameter, h is the off-axis distance of the micro-Einzel lens, and K is a positive prefactor indicating the amount of correction. With K positive, the image distance increases with increasing off-axis distance, introducing field curvature opposite to that of the micro-Einzel lens. The compensation ability of the micro-Einzel lens is obtained by calculating its image distance with ELD as a function of the lens diameter. Assuming a uniform current density in the current-limiting aperture, the FW50 spot size corresponding with a variation in image distance with respect to its axial value is calculated. The resulting sensitivity of field curvature for diameter variation is shown in Fig. 15 with the lens diameter varying from 160 μm on axis up to a maximum of 168 μm. From this graph, it is observed that for each 100 nm increase in the diameter of the micro-Einzel lens, the FW50 spot size increases by 2.3 nm. Focusing on a micro-Einzel lens at 1.1 mm from the system optical axis, the increase in its diameter that is required to compensate its field curvature is $(35\ \text{nm}/2.3\ \text{nm}) \times 100\ \text{nm} = 1.5\ \mu\text{m}$. With this result, the value of K can be determined from Eq. (9).

Astigmatism of the micro-Einzel lenses can be compensated by introducing elliptical micro-Einzel lens apertures that generate astigmatism with opposite sign.[22] Calculations on these elliptical micro-Einzel lenses are done with a charge density program.[24] It is found that the micro-Einzel lenses generate astigmatism with an approximately 30 nm FW50 disk of least confusion when the diameters of all three lens apertures in two perpendicular directions differ by 400 nm. To compensate the astigmatism of the aforementioned micro-Einzel lens, the corresponding elliptic micro-Einzel lens apertures must have a longer axis that is $(20/30) \times 400\ \text{nm} = 270\ \text{nm}$ larger compared to its shorter axis. This result determines the shape of the micro-Einzel lens at 1.1 mm from the system optical axis. The required elliptic shapes of the remaining micro-Einzel lenses in the array can now be determined: The difference in length between the two axes of the ellipses scales with the square of the ratio of the off-axis distance. The resulting elliptic MELA fully compensates astigmatism. It is remarked here that in a similar way, the SEM objective lens field curvature and astigmatism, both isotropic and anisotropic by modifying the orientation of the ellipses, can be precompensated to reduce the field aberrations of the complete 100 beam SEM.

It is important to realize here that the described compensation of astigmatism and field curvature by modifying MELA aperture shapes and sizes is influenced by the fabrication accuracy of the apertures: This accuracy determines the remaining astigmatism and defocus that can be expected. Assuming an inaccuracy of 0.25 μm in the diameter of the apertures, FW50 defocus values in the order of 50% of the geometrical spot size may be observed in the micro-Einzel lens image plane, which is considered acceptable. On the other hand, this same inaccuracy in only one direction introduces a FW50 disk of least confusion which is approximately three times larger. From these considerations, it is clear that the fabrication accuracy of the MELA is expected to be one of the limiting factors in the performance of this concept for a 100 beam SEM.

V. SUMMARY AND CONCLUSION

The performance of a MELA in a HR 100 beam SEM is limited by its field aberrations, especially astigmatism and field curvature. The contributions of these field aberrations can be reduced using an array of skewed micro-Einzel lenses, such that the apertures of each of the micro-Einzel lenses are aligned with respect to their corresponding electron beam. However, with this method, full compensation of especially astigmatism is not possible. By applying an appropriate variation of the diameter and ellipticity of the lens electrodes as a function of the off-axis distance, field curvature and astigmatism can be fully corrected. In this paper, these methods to optimize the performance of a MELA are presented. However, it is equally well possible to use these methods to improve the performance in terms of field curvature and astigmatism of the complete multibeam system, i.e., to precompensate field curvature and astigmatism of the SEM objective lens. These methods can also be used in other applications where an inclined electron beam needs to be focused by an Einzel lens.

[1] P. Kruit, Microelectron. Eng. **84**, 1027 (2007).
[2] T. H. P. Chang, D. P. Kern, and L. P. Murray, J. Vac. Sci. Technol. B **8**, 1698 (1990).
[3] A. Diebold and D. Joy, SEMATECH, 2000 (unpublished), Paper No. 00013877A-ENG, http://ismi.sematech.org/docubase/abstracts/3877aeng.htm.
[4] M. Nakasuji, S. Yoshikawa, T. Satake, and N. Noji, Jpn. J. Appl. Phys., Part 1 **44**, 5570 (2005).
[5] H. M. P. van Himbergen, M. D. Nijkerk, P. W. H. de Jager, T. C. Hosman, and P. Kruit, J. Vac. Sci. Technol. B **25**, 2521 (2007).
[6] I. L. Berry, A. A. Mondelli, J. Nichols, and J. Melngailis, J. Vac. Sci. Technol. B **15**, 2382 (1997).
[7] N. Shimazu, K. Saito, and M. Fujinami, Jpn. J. Appl. Phys., Part 1 **34**, 6689 (1995).
[8] G. I. Winograd, R. F. W. Pease, and M. A. McCord, J. Vac. Sci. Technol. B **18**, 3052 (2000).
[9] M. Mankos, S. Coyle, A. Fernandez, A. Sagle, P. Allen, W. Owens, J. Sullivan, and T. H. P. Chang, J. Vac. Sci. Technol. B **18**, 3010 (2000).

[10]E. Yin, A. D. Brodie, F. C. Tsai, G. X. Guo, and N. W. Parker, J. Vac. Sci. Technol. B **18**, 3126 (2000).
[11]H. Yasuda, S. Arai, J.-I. Kai, Y. Ooae, T. Abe, S. Maruyama, and T. Kiuchi, J. Vac. Sci. Technol. B **14**, 3813 (1996).
[12]M. Muraki and S. Gotoh, J. Vac. Sci. Technol. B **18**, 3061 (2000).
[13]E. Slot *et al.*, Proc. SPIE **6921**, 69211P (2008).
[14]M. J. van Bruggen, B. van Someren, and P. Kruit, J. Vac. Sci. Technol. B **23**, 2833 (2005).
[15]P. Kruit, Publication No. US2007029509.
[16]Y. Zhang, J. E. Barth, and P. Kruit, J. Vac. Sci. Technol. B **26**, 655 (2008).
[17]Y. Zhang and P. Kruit, Physics Procedia **1**, 553 (2006).
[18]Y. Zhang and P. Kruit, J. Vac. Sci. Technol. B **25**, 2239 (2007).
[19]B. Lencová and M. Lenc, Optik (Jena) **97**, 121 (1994).
[20]B. Lencová and G. Wisselink, ELD 3.71, electron optical design program package, 2002.
[21]P. Hawkes and E. Kasper, *Principles of Electron Optics* (Academic, London, 1996), Vol. 1, Chap. 24.
[22]Y. Zhang, M. J. van Bruggen, and P. Kruit, Patent Application No. US60/833394.
[23]B. Lencová and G. Wisselink, TRASYS 3.71, electron optical design program package, 2002.
[24]A. Henstra (private communication).